Progress In Electromagnetics Research M, Vol. 62, 11–18, 2017

Shuffling Two Quarter-Wavelength Slabs: One-Dimensional Numerical Simulation

Shin-Ku Lee[1] and Mingtsu Ho[2, *]

Abstract—An innovative idea of shuffled structure of two quarter wavelength plates is proposed in this paper, which is supported by the numerical simulation results obtained through the application of the method of characteristics (MOC). In contrast to traditional anti-reflective coatings techniques, the proposed structure is a shuffled arrangement of two quarter wavelength slabs which are in theory evenly divided into $N + 1$ and N pieces and then stacked up alternatively. These slabs are made of non-magnetic ($\mu_r = 1$) dielectric ($\varepsilon_r > 1$) materials respectively characterized by dielectric constants ε_{r1} and ε_{r2} having the relation of $\varepsilon_{r2} = (\varepsilon_{r1})^2$ to allow maximum transmission. These $2N + 1$ pieces are assembled such that there is always an ε_{r2} piece between two ε_{r1} pieces. Therefore, the proposed structure has the advantages of simple components and easy assembly. In the present simulation, the integer number N ranges from one to ten. The computational results are demonstrated in both time and frequency domains exhibiting that the proposed structure functions as a frequency selector.

1. INTRODUCTION

In terms of passive house design, many countries have developed building energy rating systems or incentive programs to decrease heat gain of the windows and encourage consumers to use high energy-efficient windows, especially for buildings with air conditioning. The addition of selected materials to windows (energy-efficient windows) is very effective in reducing solar radiation, while maintaining high transmission of visible light into buildings. Anti-reflective (AR) coatings are used to reduce reflections, being placed on the surface of optical elements such as lenses and glasses of powered telescopes, microscopes, cameras, and even for window glazing system or solar cells. For instance, the application of AR coatings in solar cells allows increasing the amount of light transmitted through the glass cover to reach the absorbing layer. Rosencrantz et al. [1] proposed an antireflective coating on both sides of a low-E glass in a double-glazed window to resolve this problem. It was able to improve light transmittance and daylight luminance and decrease the glass surface temperature. Their simulation results showed that the proposed AR low-E double-glazing system could reduce the energy demand by about 2%, compared to the low-E double-glazing system without AR coating. A comprehensive introduction of several types of AR coatings and state-of-the-art fabrication techniques was given by Raut et al. [2].

Inspired in fiber Bragg gratings [3] and using the one-dimensional method of characteristics (MOC), in this contribution, we propose an innovative interference-based coating [4] consisting of two quarter wavelength slabs equally sliced into N and $N+1$ slabs, respectively, and shuffled to form another quarter wavelength structure (see Figure 1). The proposed structure exhibits low reflection at the designed wavelength and presents the advantages of using simple components in a straightforward structure.

MOC is employed to solve Maxwell's equations and provides computational results supporting the proposed structure. MOC was first reported to generate numerical results in good agreement with

Received 20 July 2017, Accepted 22 October 2017, Scheduled 2 November 2017

* Corresponding author: Mingtsu Ho (homt@wfu.edu.tw).

[1] Research Center for Energy Technology and Strategy, National Cheng Kung University, Taiwan. [2] Graduate School of Opto-Mechatronics and Materials, Wu Feng University, Taiwan.

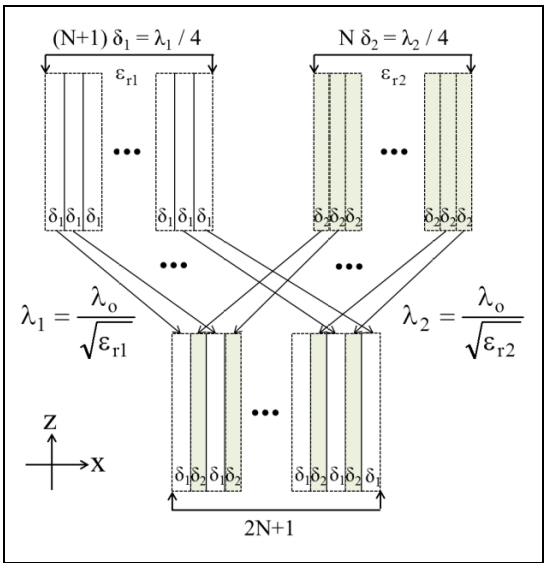

Figure 1. The proposed structure.

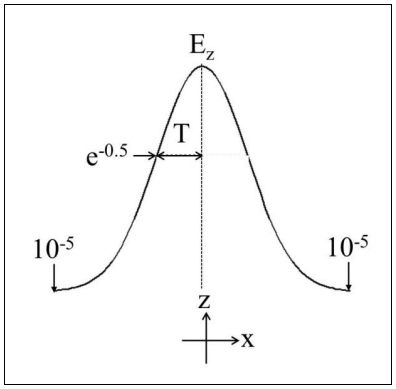

Figure 2. The incident z-polarized electric field.

those produced by the finite-difference time-domain (FDTD) technique in 1995 [5, 6]. In [4] an infinite long perfect electric conductor (PEC) strip is illuminated by a Gaussian plane electromagnetic (EM) pulse. Since then, MOC has been applied to the study of the reflection of EM fields from a traveling and/or vibrating perfect surface that is in good agreement with the theoretical values [7, 8]. In both simulations, the relativistic boundary conditions were included to account for the relativistic effects. MOC also generates numerical results showing reasonable trends in the following cases: the effects of medium conductivity on the propagation of EM fields [9] and the effects of lossless nonuniform dielectric slabs on the transmission of EM fields [10]. In recent decade, in order to overcome the grid distortion problems caused by the rotating cylinder, MOC teams up with the passing center swing back grids (PCSBG) technique in the modified O-type grid system, simulates the scattering EM fields from rotating circular cylinders, and produces numerical results that show reasonable trends [11–14].

2. GOVERNING EQUATIONS AND BOUNDARY CONDITIONS

In the numerical model, a pile of transparent sheets made of different non-magnetic transparent dielectric materials is under the illumination of a Gaussian plane EM pulse. The governing equations for the present problem are Maxwell's equations in free space [15]:

$$\frac{\partial \vec{B}}{\partial t} + \nabla \times \vec{\vec{E}} = 0, \tag{1}$$

$$\frac{\partial \vec{D}}{\partial t} - \nabla \times \vec{H} = 0, \tag{2}$$

where $\vec{\vec{E}}$ and $\vec{H}$ are the electric and magnetic field strengths, and $\vec{D}$ and $\vec{B}$ are the electric and magnetic flux densities. The electric and magnetic field strengths and flux densities are related as: $\vec{D} = \varepsilon_r \varepsilon_o \vec{E}$ and $\vec{B} = \mu_r \mu_o \vec{H}$, where ε_o and μ_o are the permittivity and permeability of free space, and ε_r and μ_r characterize the transparent materials. In the one-dimensional model, because $\vec{\vec{E}}$, $\vec{D}$, $\vec{H}$ and $\vec{B}$ are parallel to the planar boundary, and because there exist no field components along the direction of propagation, Maxwell's equations can be rewritten in a simplified version as below.

As depicted in Figure 2, the incident EM fields initially propagate in the positive-x direction, and the electric fields are polarized along the z-axis and the magnetic fields then in the negative-y direction (not shown). MOC requires a cast of Maxwell's equations into the form of Euler equation

and a coordinate transformation from the Cartesian system (t, x) to the curvilinear system (τ, ξ). The Maxwell's equations become [16]

$$\frac{\partial Q}{\partial \tau} + \frac{\partial F}{\partial \xi} = 0, \tag{3}$$

where $Q = Jq$, $F = J\xi_x f$, $q = \begin{bmatrix} B_y \\ D_z \end{bmatrix}$, $f = \begin{bmatrix} -E_z \\ -H_y \end{bmatrix}$, and $J = \left|\frac{\Delta x}{\Delta \xi}\right|$ is the Jacobian of the inverse transformation.

The partial derivative on variable F in Eq. (3) is replaced by the central difference operator which is defined as [15]

$$\delta_k(F) = (F)_{k+\frac{1}{2}} - (F)_{k-\frac{1}{2}}, \tag{4}$$

where the cell indexing k designates the grid cell center, and the one-half indexing indicates the interface between cells. Therefore, Equation (4) computes the change of F for the kth cell, i.e., the flux difference between the two interfaces. It is understood that MOC evaluates the flux and solves the flux difference for every cell. With Eq. (4) and finite difference operator (Δ), Eq. (3) becomes [16]

$$\frac{Q^{n+1} - Q^n}{\Delta \tau} + \frac{\delta_i F}{\Delta \xi} = 0. \tag{5}$$

Note that the two denominators of Eq. (5) are the finite difference approximations in time and space, respectively. The first term of Eq. (5) is the approximation of the temporal derivative of the variable Q which has two superscripts $(n + 1)$ and (n) representing the two successive numerical time-steps. The second term is the spatial derivative of the variable F. To solve the system of equations, the flux vector splitting technique [16] and lower-upper approximate factorization scheme [17] are employed.

Since the EM fields propagate through a pile of clear sheets made of two different dielectric materials, there are three types of boundary: air-dielectric, dielectric-air, and dielectric-dielectric. The proper boundary conditions are as follows. Across the interface, both electric and magnetic field strengths must be continuous. At the outermost boundaries of the numerical model, the appropriate boundary conditions ensure that the departing EM fields keep propagating outward.

3. THE PROPOSED STRUCTURE

Illustrated in Figure 1 are the two quarter wavelength plates that are uniformly divided into $(N + 1)$ and (N) pieces and then shuffled to form a structure of $(2N + 1)$ components. Providing that in free space the wavelength λ_o of interest is under investigation, two materials are respectively characterized by the dielectric constant and thickness: $(\varepsilon_{r1}, \delta_1)$ and $(\varepsilon_{r2}, \delta_2)$, the following relations hold

$$\delta_1 = \frac{\lambda_1}{4(N+1)}, \tag{6}$$

$$\delta_2 = \frac{\lambda_2}{4(N)}, \tag{7}$$

where

$$\lambda_1 = \frac{\lambda_o}{\sqrt{\varepsilon_{r1}}}, \tag{8}$$

and

$$\lambda_2 = \frac{\lambda_o}{\sqrt{\varepsilon_{r2}}}, \tag{9}$$

are the wavelengths of the transmitted EM fields inside two media, respectively [18]. In relating the index of refraction (n) to the relative permittivity (ε_r) we have

$$n = \sqrt{\varepsilon_r}. \tag{10}$$

In order to have maximum transmission between these two materials, ε_{r1} and ε_{r2} are selected to have the following relationship [19]

$$\varepsilon_{r1} \approx \sqrt{\varepsilon_{r2}}. \tag{11}$$

Further descriptions regarding the proposed structure are as follows: N can be any positive integer number; both δ_1 and δ_2 can be very small numbers and dependent on N and the wavelength of interest. For the present study, N is set to vary from 1 to 10 corresponding to total numbers of transparent sheets of the proposed structure, 3 and 21.

4. THE PROBLEM

The schematic diagram of the incident Gaussian EM pulse is depicted in Figure 2 where only the electric field intensity is shown. The initial position of the peak of the incident EM pulse is set to 100 nm measured from the structure. For practical reasons, the z-polarized incident electric field strength has a maximum magnitude of one volt per meter and a width of $T = 69.466$ attoseconds measured from the peak to the level of $\exp(-0.5)$ which is below the known extreme ultraviolet pulse laser [20]. The Gaussian pulse has a cut-off level of 10^{-5} V/mat both ends, and the highest frequency content in spectrum is about 11×10^{15} Hz corresponding to a shortest wavelength of 27 nm, beyond the visible light range. The visible light spectrum is referred to a frequency range approximately from 420 to 770 THz corresponding to a wavelength range from 390 to 720 nm.

Numerical discretization typically causes discrepancies of the experimental numbers from the actual values since no fractional grid point is acceptable. Provided that the two dielectric constants are $\varepsilon_{r1} = 1.5$ and $\varepsilon_{r2} = (\varepsilon_{r1})^2 = 2.25$ and that two wavelengths (λ_o) of interest are 390 and 720 nm, summarized in Tables 1 and 2 are two sets of numbers used in the numerical model with respect to various N values. Each table consists of four cases, namely $N = 1$, 3, 5 and 10. All numbers listed are based on the grid density of ten points per nanometer in order to have as close as possible integer numbers of points to represent δ_1 and δ_2. Note that two symbols λ' and λ'_o are the numerical wavelengths respectively inside media and in free space based upon the close space discretization, which show the discrepancies of the numbers used in the model from the actual values.

Table 1. Settings for various proposed structure ($\lambda_o = 390$ nm).

N	$\varepsilon_{r1} = 1.5$; $\lambda_1 = 318.43$ nm			$\varepsilon_{r2} = 2.25$; $\lambda_2 = 260.00$ nm		
	δ_1 (nm)	λ'_1 (nm)	λ'_{o1} (nm)	δ_2 (nm)	λ'_2 (nm)	λ'_{o2} (nm)
1	39.80	318.40	389.96	65.00	260.00	390.00
3	19.90	318.40	389.96	21.70	260.40	390.60
5	13.30	319.20	390.94	13.00	260.00	390.00
10	7.20	316.80	388.00	6.50	260.00	390.00

Table 2. Settings for various proposed structure ($\lambda_o = 720$ nm).

N	$\varepsilon_{r1} = 1.5$; $\lambda_1 = 587.88$ nm			$\varepsilon_{r2} = 2.25$; $\lambda_2 = 480.00$ nm		
	δ_1 (nm)	λ'_1 (nm)	λ'_{o1} (nm)	δ_2 (nm)	λ'_2 (nm)	λ'_{o2} (nm)
1	73.50	588.00	720.15	120.00	480.00	720.00
3	36.80	588.80	721.13	40.00	480.00	720.00
5	24.50	588.00	720.15	24.00	480.00	720.00
10	13.40	589.60	722.11	12.00	480.00	720.00

5. NUMERICAL RESULTS

Multi-reflection/transmission phenomenon is expected to be observed when the EM fields propagate onto a stack of dielectric sheets. Figures 3 and 4 gather several snapshots of the electric fields at different time instances along the computational domain for $\lambda_o = 390$ and 720 nm, respectively. It is

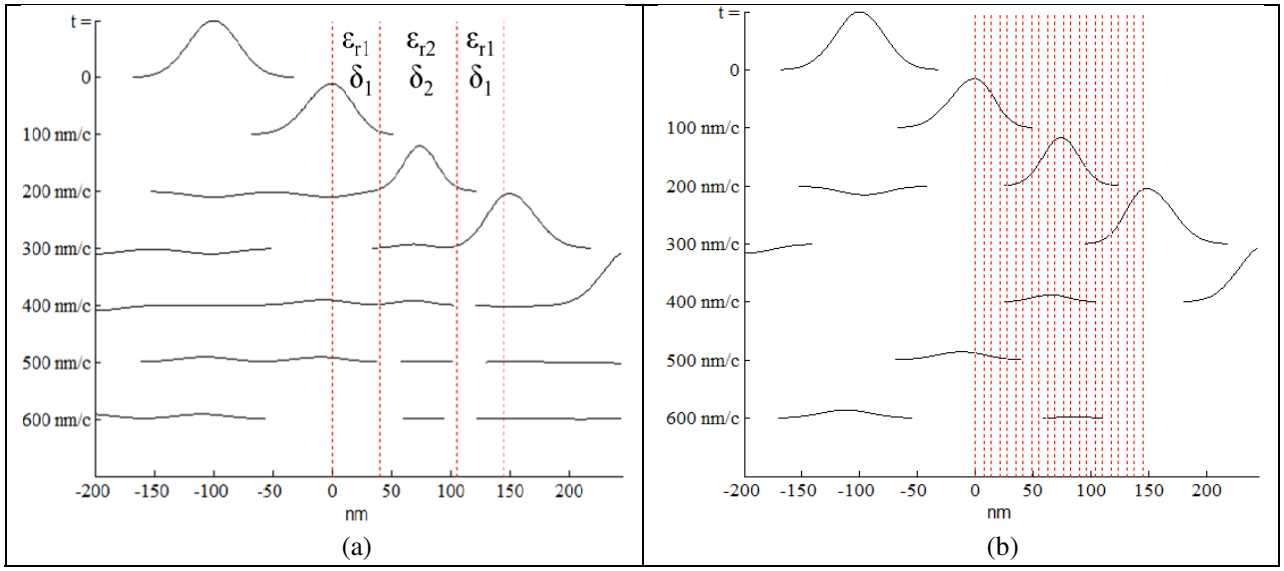

Figure 3. EM fields propagate onto structure ($\lambda_o = 39\,\text{nm}$) with (a) $N = 1$, (b) $N = 10$.

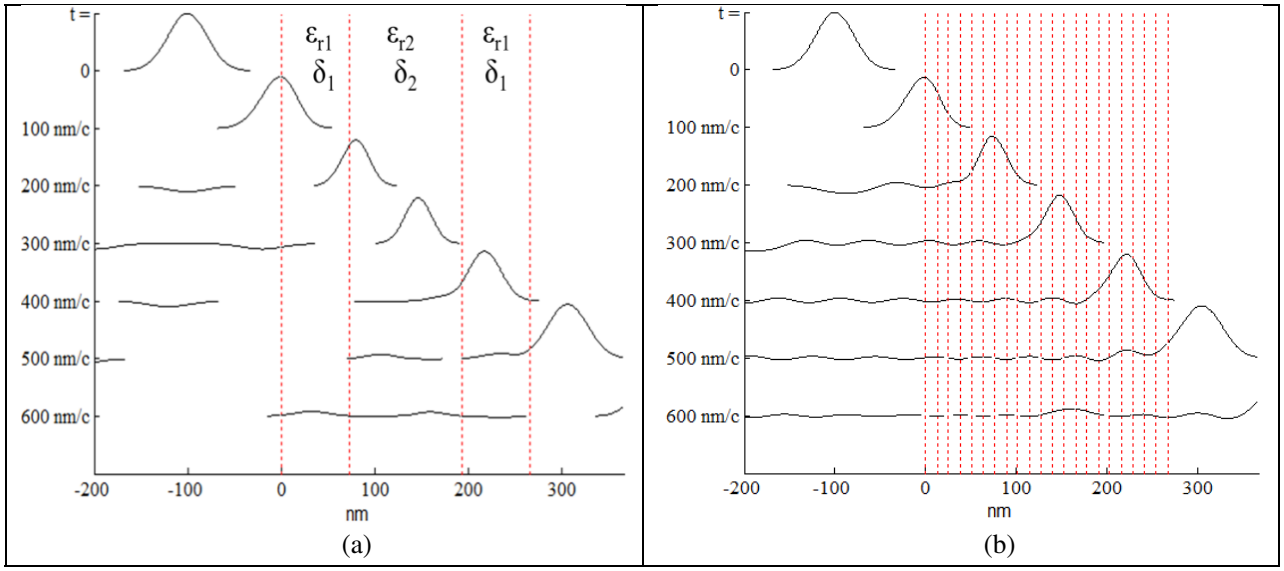

Figure 4. EM fields propagate onto structure ($\lambda_o = 720\,\text{nm}$) with (a) $N = 1$, (b) $N = 10$.

noted that the time axis is in the units of nm/c where c is the speed of light, that only magnitude greater than 5×10^{-3} is shown, and that EM fields experience multi-reflection/transmission when they propagate through the proposed structures.

The reflected electric fields are recorded as functions of time and illustrated in Figure 5 for two different wavelengths. It can be clearly observed that the reflectivity of both cases is dependent on the number N, that the primary reflections are reversed which are reflected from the front edge of structure, that the secondary reflections are upright which are reflected from the other edge of structure, and that the magnitudes of reflected ripples between two main reflections decrease as N increases and tend to be null after the secondary which supports the fact that the proposed structures allow maximum transmission.

In Figure 5(a) for $N = 1$ case (dashed line), the incidence seems to propagate onto a medium having a refractive index of $\sqrt{\varepsilon_{r1}}$, the reversed peak value of the reflected electric field is close to $-0.1\,\text{V/m}$

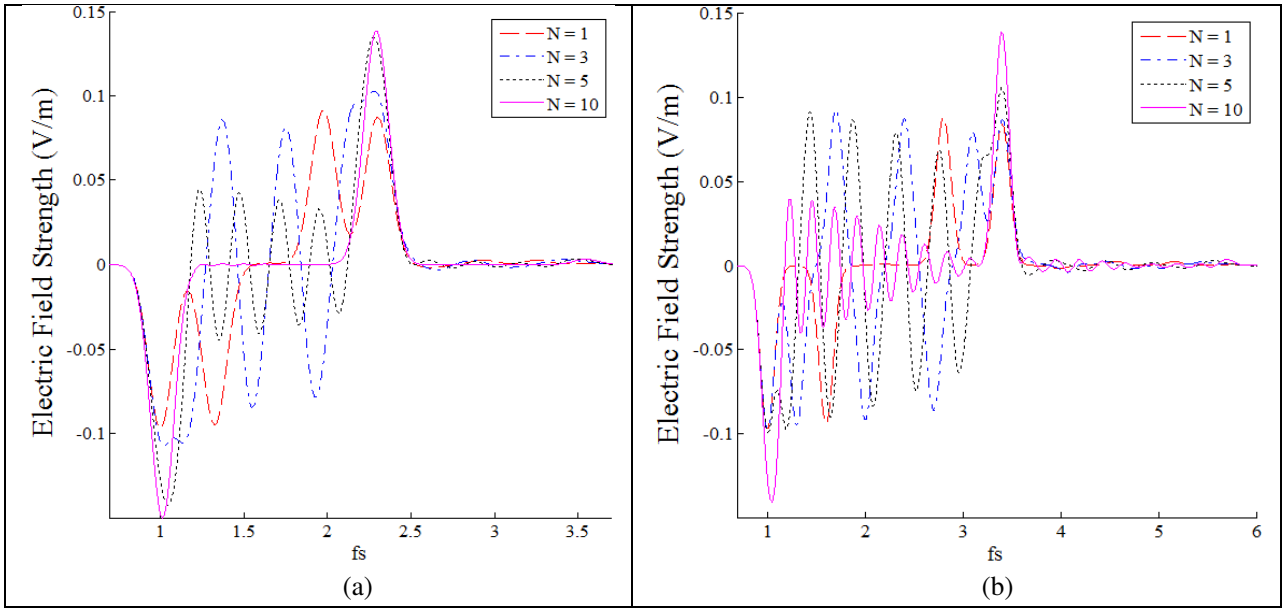

Figure 5. Reflected electric fields (a) $\lambda_o = 390\,\text{nm}$, (b) $\lambda_o = 720\,\text{nm}$.

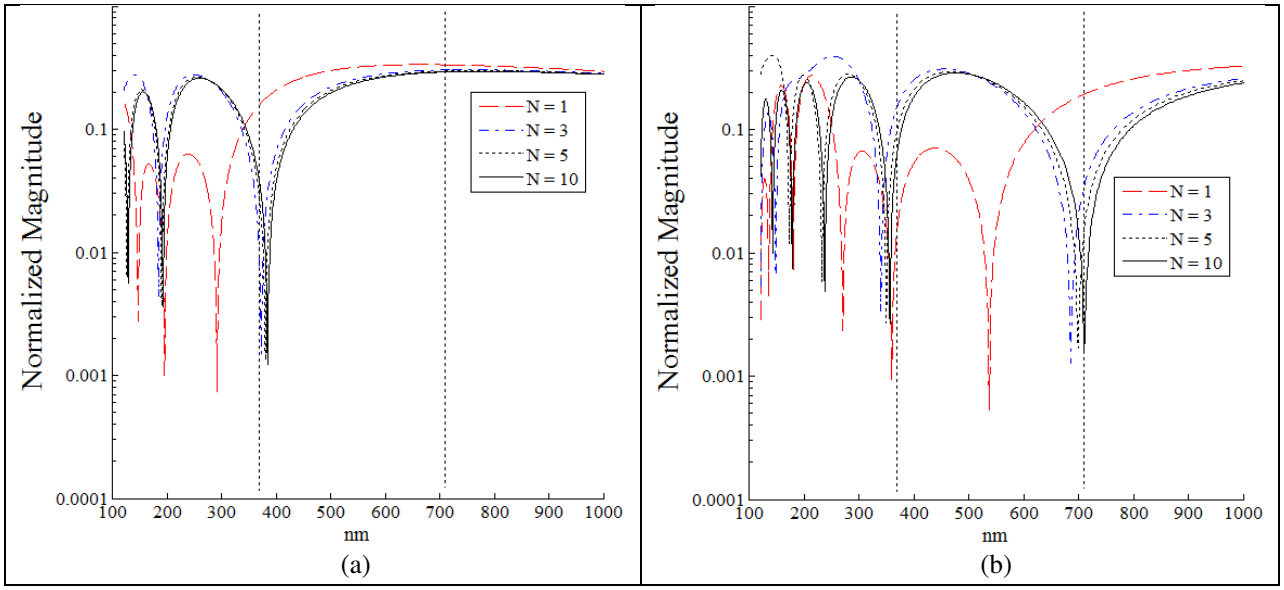

Figure 6. Spectrum of reflected electric fields (a) $\lambda_o = 390\,\text{nm}$, (b) $\lambda_o = 720\,\text{nm}$.

since δ_1 is relatively thick. Also observed is that the magnitude of the reversed peak increases as N increases. The $N = 10$ case (solid line) has a minimum magnitude is about $-0.15\,\text{V/m}$ corresponding to an equivalent refractive index which is about the geometric mean of the two refractive indices. Similar observations can be found in Figure 5(b). In $\lambda_o = 720\,\text{nm}$ case because the slice thicknesses are thicker than those in $\lambda_o = 390\,\text{nm}$ case, the magnitudes of reflected ripples between two peaks are relatively bigger and decrease as the EM pulse propagate farther inside structure. This phenomenon becomes more significant when $N = 10$.

Further numerical evidence supporting the proposed idea is illustrated in Figure 6 and two sets of

spectrum corresponding to the reflected electric fields in Figure 5 respectively. Both $N = 1$ cases bear the largest deviation from the designed wavelength, whose minimum reflections occur at the location about 75% of λ_o and are estimated to be 293 and 540 nm, respectively. It is clearly found that the $N = 10$ case has the best result of four where the minimum reflection almost coincide with the designed wavelength. It has been shown that the proposed structures function as anti-reflection slabs near the designed wavelength and that better results can be obtained by increasing the integer number N.

6. CONCLUSION

The innovative shuffled structure of two quarter wavelength slabs has been proposed and numerically proved through the application of the method of characteristics, which has the advantages that components are simple and identical in thickness and easy to synthesize compared to the traditional anti-reflective coating techniques. The computational results exhibit the proposed structure functions as antireflective slab and are demonstrated in both time and frequency domains. It is also pointed out that the deviation of the computational results from the desired values is caused by the discretization process. The future study includes simulations for other types of formations and more complicated configurations for different purposes.

ACKNOWLEDGMENT

The gratitude of the authors is expressed to the Ministry of Science and Technology of Taiwan for their financial support of this paper under project MOST 106-3113-E-006-006-CC2.

REFERENCES

1. Rosencrantz, T., H. Bulow-Hube, B. Karlsson, and A. Roos, "Increased solar energy and daylight utilization using anti-reflective coating in energy-efficient windows," *Sol. Energy Mater. Sol. Cells*, Vol. 89, 249–260, 2005.
2. Raut, H. K., V. A. Ganesh, A. S. Nairb, and S. Ramakrishna, "Anti-reflective coatings: A critical, in-depth review," *Energy & Environmental Science*, Vol. 4, 3779–3804, 2011.
3. Hill, K. O., Y. Fujii, D. C. Johnson, and B. S. Kawasaki, "Photosensitivity in optical fiber waveguides: Application to reflection fiber fabrication," *Appl. Phys. Lett.*, Vol. 32, No. 10, 647, 1978.
4. MacLeod, H. A., *Thin Film Optical Filters*, 3rd Edition, CRC, 2001.
5. Taflove, A., *Computational Electrodynamics, The Finite-Difference Time-Domain Method*, Artech House, Boston, 1995.
6. Donohoe, J. P., J. H. Beggs, and M. Ho, "Comparison of finite-difference time-domain results for scattered EM fields: Yee algorithm vs. a characteristic based algorithm," *27th IEEE Southeastern Symposium on System Theory*, March 1995.
7. Ho, M., "Scattering of EM waves from traveling and/or vibrating perfect surface: Numerical simulation," *IEEE Transactions on Antennas and Propagation*, Vol. 54, No. 1, 152–156, January 2006.
8. Ho, M., "EM scattering from PEC plane moving at extremely high speed: simulation in one dimension," *Journal of Applied Science and Engineering (JASE)*, Vol. 17, No. 4, 429–436, December 2014.
9. Ho, M. and F.-S. Lai, "Effects of medium conductivity on electromagnetic pulse propagation onto dielectric half space: One-dimensional simulation using characteristic-based method," *Journal of Electromagnetic Waves and Applications*, Vol. 21, No. 13, 1773–1785, 2007.
10. Ho, M., F.-S. Lai, S.-W. Tan, and P.-W. Chen, "Numerical simulation of propagation of EM pulse through lossless non-uniform dielectric slab using characteristic-based method," *Progress In Electromagnetic Research*, Vol. 81, 197–212, 2008.

11. Ho, M., "Numerically solving scattered electromagnetic fields from rotating objects using passing center swing back grid technique: A proposal," *Journal of Electromagnetic Waves and Applications*, Vol. 23, No. 23, 389–394, January 2009.
12. Ho, M., "Simulation of scattered fields from rotating cylinder in 2D: Under illumination of TE and TM gaussian pulses," *PIERS Proceedings*, Moscow, Russia, August 18–21, 2009.
13. Ho, M., "Simulation of scattered EM fields from rotating cylinder using passing center swing back grids technique in two dimensions," *Progress In Electromagnetic Research*, Vol. 92, 79–90, 2009.
14. Ho, M., L.-A. Tsai, and C.-J. Tsai, "EM fields inside a rotating circular hollow dielectric cylinder: Numerical simulation in 2Ds," *Progress In Electromagnetics Research M*, Vol. 45, 1–8, 2016.
15. Harrington, R. F., *Time-harmonic Electromagnetic Fields*, McGraw-Hill, New York, 1961.
16. Whitfield, D. L. and M. Janus, "Three-dimensional unsteady euler equations solution using flux vector splitting," AIAA Paper No. 84-1552, June 1984.
17. Briley, W., S. Neerarambam, and D. Whitfield, "Implicit lower-upper/approximate-factorization algorithms for viscous incompressible flows," *12th Computational Fluid Dynamics Conference, Fluid Dynamics and Co-located Conferences*, A95-36593, San Diego, CA, U.S.A., 1995.
18. Orfanidis, S. J., *Electromagnetic Waves and Antennas*, ECE Department, Rutgers University, New Jersey, U.S.A., 2016.
19. Krepelka, J., "Maximally flat antireflection coatings," *Jemná Mechanika A Optika*, Vol. 3–5, 53–56, 1992.
20. Chang, H.-T., M. Zürch, P. M. Kraus, L. J. Borja, D. M. Neumark, and S. R. Leone, "Simultaneous generation of sub-5-femtosecond 400 nm and 800 nm pulses for attosecond extreme ultraviolet pump — Probe spectroscopy," *Optics Letters*, Vol. 41, No. 22, 5365–5368, 2016.